Quantifying the average and the likelihood of increases in space weather indices and in situ measurements during Solar Cycles 20–23

Whitney Q. Lohmeyer* and Anthony Pang

Department of Aeronautics and Astronautics,
Massachusetts Institute of Technology,
Cambridge, MA, 02139, USA
E-mail: wqlohmey@mit.edu
E-mail: apang90@gmail.com
*Corresponding author

Kerri Cahoy

Department of Aeronautics and Astronautics,
Massachusetts Institute of Technology,
Cambridge, MA, 02139, USA
and
Department of Earth Atmospheric and Planetary Sciences,
Massachusetts Institute of Technology,
Cambridge, MA, 02139, USA
E-mail: kcahoy@mit.edu

Yuri Shprits

Department of Earth Atmospheric and Planetary Sciences,
Massachusetts Institute of Technology,
Cambridge, MA, 02139, USA
and
Department of Earth and Space Sciences,
University of California Los Angeles,
Los Angeles, CA 90095, USA
and
Skolkovo Institute of Science and Technology,
Odintsovsky District, Moscow Region, 143025, Russia
E-mail: shprits@mit.edu

Abstract: It is known that space weather harshly affects spacecraft performance, yet spacecraft operations and understand the cause of anomalies can be challenging due to the complexity of environmental metrics. In this work, we analyse five metrics and in-situ measurements (Kp, Dst, and AE index, and high-energy proton and electron flux) throughout Solar Cycles 20–23 (1964 to 2008), and provide a baseline for the environment during the phases of the solar cycles (maximum, minimum, declining or ascending). We define increased activity as activity greater than two median absolute deviations (MADs) above the average activity for each phase. MAD is used, rather than

standard deviation, because it is more resilient to outliers. The average and MAD values are tabulated in Table 3 to Table 6. We determine the probability that increased activity occurs 3, 14 or 30 days before a random day to distinguish between increased/quiet activities and to aid in correlating intensifications of the environment and anomalous satellite performance.

Keywords: satellite anomalies; radiation effects; space weather indices; space weather measurements.

Reference to this paper should be made as follows: Lohmeyer, W.Q., Pang, A., Cahoy, K. and Shprits, Y. (xxxx) 'Quantifying the average and the likelihood of increases in space weather indices and in situ measurements during Solar Cycles 20–23', *Int. J.* Space Science and Engineering, Vol. X, No. Y, pp.000–000.

Biographical notes: Whitney Q. Lohmeyer received her BS in Aerospace Engineering from North Carolina State University in 2011, and her MS in Aerospace Engineering from MIT in 2013, and will obtain her PhD in Aerospace Engineering from MIT in 2015. She is an NSF Graduate Research Fellow and an NASA Space Grant Recipient. Her research investigates the impacts of the space radiation environment on satellite electronics.

Anthony Pang is a Systems Engineer in the Survivability and Vulnerability Group and ESD Laboratory Supervisor at Boeing Space & Intelligence Systems. He received his BEng (2011) in Mechanical Engineering from the City College of New York, and SM (2013) in Aerospace Engineering from the Massachusetts Institute of Technology, working in the Space Propulsion Laboratory. His work involves satellite radiation modelling and design, on-orbit contamination analysis, electric propulsion simulations, and electrostatic discharge experimentation. He has received a National Science Foundation Graduation Research Fellowship for his graduate work on plasma-surface interaction diagnostics and cusped-field plasma thrusters design.

Kerri Cahoy received her BS in Electrical Engineering from Cornell University in 2000, and her MS in Electrical Engineering from Stanford University in 2002, and her PhD in Electrical Engineering from Stanford University in 2008. After working as a Senior Payload and Communications Sciences Engineer at Space Systems Loral, she competed a NASA Postdoctoral Programme Fellowship at NASA Ames Research Center and held a research staff appointment with MIT/NASA Goddard Space Flight Center. She is currently a Boeing Assistant Professor in the MIT Department of Aeronautics and Astronautics with a joint appointment in the Department of Earth, Atmospheric, and Planetary Sciences at MIT.

Yuri Shprits studies the dynamics of the energetic particle populations. His research involves modelling, data assimilation, mission design and modelling of the effects of radiation on satellites. He developed modelling and data assimilation tools that allow assimilation of 3D data from multiple spacecraft. He has quantified the effects of scattering by ELF/VLF/ULF waves. He has been awarded the Presidential Early Career Awards for Scientists and Engineers in 2012 and Arne Richter Award for Outstanding Young Scientists, of the European Geosciences Union, Vienna, Austria in 2011. Google scholar lists 171 publications for him, 2080 citations, h-index is 26.

1 Introduction

It is widely acknowledged that space weather affects spacecraft operations and contributes to anomalous satellite performance (e.g., Baker, 2000; Fennell et al., 2001; Iucci et al., 2006; Allen, 2010; Bodeau, 2010). Understanding the causal effects of space weather on satellite performance requires a thorough understanding of the space weather environment and the frequency and likelihood of hazardous space weather events. When spacecraft anomalies occur, the time series of the anomaly is often compared to the conditions of the radiation environment. When determining if the environment contributed to the anomaly, the definitions of the space weather metrics must be understood, as well as their average values during particular periods of the solar cycle and what constitutes as elevated, quiet, or spontaneous jumps in the space environment data. Once these values are properly compared, a relationship could be determined between a particular space weather metric and an anomaly occurs.

In this study, we use data from Solar Cycles 20–23 (years 1964 to 2008) and quantify the average and median absolute deviation (MAD) to first quantify the average value of five space weather metrics and in situ measurements for each phase of the solar cycle, and to determine in which phase of the solar cycle metrics are statistically more likely to increase above their average value. It is important to understand that increases in the metrics do not necessarily mean that the metrics are elevated, just that the metric increases compared to the average metric for that phase. We partition each 11-year solar cycle into four phases: solar maximum, declining, solar minimum, and ascending phases, and analyse the following metrics: Disturbance storm time index (Dst), Kp index, Auroral Electrojet (AE) index and high-energy protons (10 MeV). We also analyse the $\log_{10}$ (1.8–3.5 MeV) electron flux, but the Los Alamos National Lab (LANL) electron flux data set referenced in this study only extends from 1989 to 2009. The electron measurements analysed in this study, $\log_{10}$ (1.8–3.5 MeV Electron flux), can be approximated as equal to 2 MeV electron flux for the purposes of understanding the effects of space environment on satellite performance.

The sunspot number is the longest available quantitative record of solar activity, and serves as the parameter used to monitor and define the solar cycle (Clette et al., 2007). The sunspot number is determined from eye- and camera-based observations of relatively cooler/darker regions on the sun, known as sunspots (Vaquero, 2007).

As shown in Table 1, Solar Cycles 20–23 are not all 11 years long, but 13, 11, 11, and 13 years, respectively. Therefore, rather than partitioning the cycles into four equal phases, we base our definition of phases on the solar cycle start and end year, and solar maximum defined by Kane (2002), as shown in Table 1. The period of solar maximum, shown in Table 2, is defined as the period one-year before and one year after the year of solar maximum in Kane's (2002) study. The ascending periods of the solar cycle are defined as the number of years before the period of solar maximum; this ranges from two to three years depending on the overall length of the solar cycle. Solar minimum is the last three years of the cycle, also captured in Kane (2002), and the declining phase is the period of time between the solar maximum and solar minimum phases. The periods of time for these partitioned phases are given in Table 2.

Table 1 Solar cycle definition

Solar cycle number	*Start year*	*End year*	*Solar maximum year*
20	1964	1976	1968
21	1976	1986	1979
22	1986	1996	1989
23	1996	2008	2000

Source: Kane (2002)

Table 2 Solar cycle partitioned periods for Solar Cycles 20–23

Solar cycle number	*Ascending period*	*Solar maximum period*	*Declining period*	*Solar minimum period*
20	1964–1966	1967–1969	1970–1973	1974–1976
21	1976–1977	1978–1980	1981–1983	1984–1986
22	1986–1987	1988–1990	1991–1993	1994–1996
23	1996–1998	1999–2001	2002–2005	2006–2008

2 Space environment activity and metrics

The following subsections introduce and define the five space environment metrics and in situ measurements considered in this analysis.

2.1 Auroral Electrojet

The AE index represents electric currents, which travel around the E region of the Earth's ionosphere near the Northern and Southern Polar Circles (Kamide and Akasofu, 1983). The AE is due to Hall currents (perpendicular to the Earth magnetic field) induced by the Earth's magnetic field and the electric fields present in the ionosphere. While relatively unperturbed during magnetic quiet periods, the electrojet increases in strength during disturbed periods and expands to both higher and lower latitudes, which is a result of enhanced particle precipitation and enhanced ionospheric electric fields (Neil and Sugiura, 1966). Thus, the AE index is an indicator of severe surface charging for satellites in the low Earth orbit (LEO) altitudes (less than approximately 600 km), but is not a primary index used for geostationary satellites.

2.2 Disturbance storm time index

The Dst measures the hourly average of the global variation in the horizontal component of the Earth's magnetic field, and is used to indicate the strength of the ring current around Earth (Fennell et al., 2001). This ring current is formed primarily by protons from drifts due to the magnetic field gradient and curvature, and induces a magnetic field counter to that of the Earth's that in turn weakens the Earth's magnetic field. A negative Dst value indicates that Earth's magnetic field is weakened. The weakening of the Earth's magnetic field is also the main defining property of a geomagnetic storm (Gonzalez et al., 1994; Mursula et al., 2008).

2.3 Kp index

While Dst serves to quantitatively describe the strength of geomagnetic activity, the Kp index is a general planetary index constructed from ground-based magnetometers at various geomagnetic latitudes that qualitatively characterises geomagnetic activity (Horne et al., 2013). The scale ranges from zero to nine, where nine designates the highest level of severity for geomagnetic storms (O'Brien, 2009). The Kp index, while often challenging to interpret, is also used as a proxy for surface charging and magnetospheric convection (Thomsen, 2004). Magnetospheric convection causes low-energy electron flux to increase at geostationary orbit (Fennell et al., 2001), and is often used to characterise relativistic electron activity.

2.4 High-energy protons

High-energy protons can enter into the Earth's magnetosphere at the poles, make contact with other particles, and produce electron and ion pairs that temporarily increase the plasma density in the lowest region of the ionosphere (Baker, 2000, 2002). This causes absorption of short wave radio signals and widespread blackout of communications, sometimes called a polar cap absorption event. Radiation from the accumulation of high-energy protons can also damage spacecraft electronics, degrade solar arrays, cause single event upsets, and pose a serious threat to the safety of astronauts.

2.5 High-energy electrons

High-energy electrons with energies > 1 MeV can cause deep dielectric charging when they penetrate the surface of a satellite and deposit into the spacecraft's dielectric materials, including cables, conductors and electronics. If dielectric charging occurs at a rate greater than the existing charge can escape from the dielectric, then a dielectric discharge can occur (Baker, 2000; Fennell et al., 2001; Bodeau, 2010). Differential charging can also cause electrical shorts or malfunctions and lead to major satellite component failures. These high-energy electrons are at a maximum during the declining phase of the solar cycle, when high-speed solar wind streams occur (Shea and Smart, 1998; Miyoshi and Kataoka, 2008). Studies indicate that internal discharge event occurrence peaks near local noon in contrast to surface charging which peaks between midnight and dawn (Fennell et al., 2001). Fennell et al. (2001) also suggest that susceptibility to internal charging is largely a function of spacecraft shielding and orbit; satellites that spend long periods of time in high flux regions require thicker shielding.

3 Method: statistical analysis of the space environment

The Kp, AE, Dst and 10 MeV Proton flux data has been gathered from the OMNI2 dataset from 1963 to 2012 (King and Papitashvili, 2013). This dataset does not contain electron flux values, so electron flux data from LANL charged particle instruments for years of 1989 to 2009 were also gathered (Reeves et al., 2011). For these time periods, we calculate the mean and MAD for each dataset. Given the skewedness of the data, as seen in Figure 1, it is inappropriate to assume that the resulting distributions will be

Gaussian and, from the Jarque-Bera normality test, it has been empirically determined that none of the data has a normal distribution.

Thus, using standard deviation to characterise the variability of the data is not as reliable of a statistical indicator as other more robust statistical indicators. In the case of a skewed distribution, the MAD is more resilient to outliers in data than the standard deviation, because for the standard deviation the distances from the mean are squared and the large outliers are weighted more heavily and can potentially skew the results (Draghici, 2001).

Figure 1 Distribution of the daily average values of Kp index for solar minimum of Cycle 23 (see online version for colours)

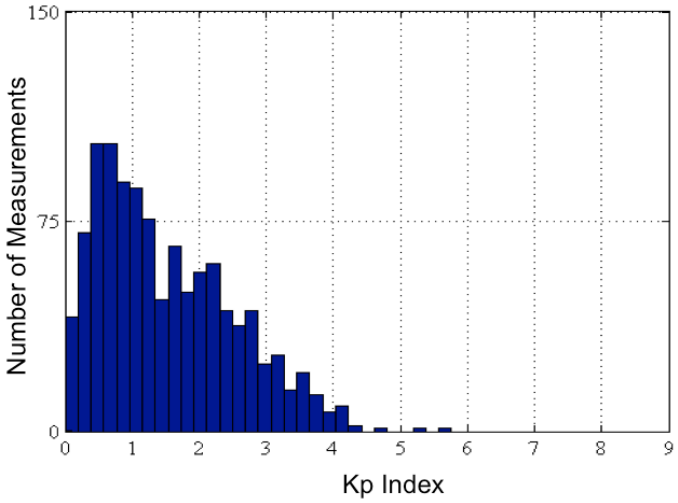

Notes: The skewed distribution of Kp is not Gaussian, which means a more robust indicator, other than mean and standard deviation based on a Gaussian distribution, is needed. The Jarque-Bera normality test returned an h value of 1, which indicates that these are not normal distributions.

Table 3 Solar Cycle 20 (1964–1976)

	Ascending period	*Solar maximum period*	*Declining period*	*Solar minimum period*
Kp mean	1.740	2.094	2.049	2.538
Kp MAD	1.033	1.087	1.074	1.168
AE mean	128.149	193.557	195.498	251.339
AE MAD	101.142	139.052	142.135	173.504
Dst mean	–2.431	–13.628	–16.639	–12.782
Dst MAD	10.690	15.055	14.258	13.137
10 MeV proton mean	N/A	5.690	19.325	0.852
10 MeV proton MAD	N/A	9.846	36.228	0.994
Log_{10} (1.8–3.5) MeV electron flux mean	N/A	N/A	N/A	N/A
Log_{10} (1.8–3.5) MeV electron flux MAD	N/A	N/A	N/A	N/A

In comparison, for the computation of the MAD, the magnitude of a relatively small number of outliers is irrelevant and will not skew the results. MAD is computed by finding the median of the absolute residuals:

$$\text{MAD} = \text{median}\left(\left|X_i - \text{median}_j\left(X_j\right)\right|\right) \quad (1)$$

where i is a unit in the set and j is the median of the set. Therefore, utilising a MAD methodology can eliminate the need to subjectively eliminate outliers from the dataset.

Table 4 Solar Cycle 21 (1976–1986)

	Ascending period	*Solar maximum period*	*Declining period*	*Solar minimum period*
Kp mean	2.188	2.341	2.810	2.450
Kp MAD	1.047	1.098	1.159	1.112
AE mean	N/A	213.074	271.239	228.802
AE MAD	N/A	155.661	183.932	162.365
Dst mean	–15.261	–16.632	–21.652	–16.243
Dst MAD	12.689	17.653	20.490	14.020
10 MeV proton mean	1.037	7.456	5.049	1.507
10 MeV proton MAD	1.293	13.258	8.494	2.288
Log_{10} (1.8–3.5) MeV electron flux mean	N/A	N/A	N/A	N/A
Log_{10} (1.8–3.5) MeV electron flux MAD	N/A	N/A	N/A	N/A

Table 5 Solar Cycle 22 (1986–1996)

	Ascending period	*Solar maximum period*	*Declining period*	*Solar minimum period*
Kp mean	2.119	2.520	2.672	2.260
Kp MAD	1.010	1.125	1.184	1.134
AE mean	187.963	238.064	251.950	210.650
AE MAD	139.418	177.094	182.717	158.862
Dst mean	–13.681	–23.555	–22.843	–16.306
Dst MAD	13.558	20.777	20.431	13.720
10 MeV proton mean	0.735	25.849	10.025	1.049
10 MeV proton MAD	0.753	47.381	17.474	0.662
Log_{10} (1.8–3.5) MeV electron flux mean	N/A	N/A	–0.469	–0.220
Log_{10} (1.8–3.5) MeV electron flux MAD	N/A	N/A	0.655	0.705

Table 3 to Table 6 contain the mean and MAD for the metrics used in this study for Solar Cycles 20, 21, 22, and 23, respectively. With the aggregate data from each solar cycle, we determined the average value and MAD of each space weather metric and in situ measurement. These values were then used to determine that probability of increases greater than two MAD s above the average value occurring within the aforementioned phases (the solar maximum, descending, minimum, and ascending phases). This approach

provides greater insight for the satellite operator and engineering community into baselining how space weather activity changes throughout the solar cycle. Understanding whether sudden jumps in a given metric are typical for a particular phase of the solar cycle is particularly useful for determining the contribution of the environment on component anomalies. We note that the purpose of this paper is not to discover in which phase the metrics are most increased, as this is well understood (Russell and McPherron, 1973; Miyoshi and Kataoka, 2008), but rather to provide a means for characterising and comparing space weather activity.

Table 6 Solar Cycle 23 (1996–2008)

	Ascending period	*Solar maximum period*	*Declining period*	*Solar minimum period*
kp mean	1.845	2.204	2.407	1.518
Kp MAD	1.001	1.118	1.187	1.018
AE mean	178.751	218.946	247.812	133.286
AE MAD	136.641	162.697	179.411	111.253
Dst mean	–14.129	–16.606	–20.807	–6.921
Dst MAD	12.578	18.241	16.721	8.836
10 MeV proton mean	3.077	18.633	17.780	2.357
10 MeV proton MAD	4.457	34.256	32.628	4.269
Log_{10} (1.8–3.5) MeV electron flux mean	–0.627	–0.620	–0.240	–0.215
Log_{10} (1.8–3.5) MeV electron flux MAD	0.594	0.585	0.592	0.628

Table 7 Summary of phase averages and MAD values for the five metrics and in situ measurements

Metric/measurement	*Min phase average*	*Max phase average*	*Min MAD*	*Max MAD*
Kp	1.518	2.810	1.001	1.187
Dst (nT)	–22.555	–2.431	8.835	20.777
AE	128.149	271.238	101.142	183.932
10 MeV proton flux (pfu)	0.735	25.849	0.753	47.381
Log_{10} (1.8–3.5 MeV electron flux)	–0.627	–0.215	0.585	0.705

4 Results

In Section 4.1, we describe our analysis of the annual averages of the space weather activity from 1963 to 2012. In Section 4.2, we discuss the same approach applied for each of the four shorter period phases of space weather activity from Solar Cycle 20–23 (1964 to 2008); these results are tabulated in Tables 3 to 6. We consider shorter periods of time in Section 4.3, where we describe the likelihood that increased activity occurs some number of days before the first day of each month per year (3 days, 14 days, and 30 days) within each of the four phases of the solar cycle. Increased activity is defined as greater than 2 MAD.

4.1 Annual average values of space weather activity between 1963 to 2012

To understand the variability of the space environment with respect to the solar cycle, we calculate the annual average value of the five space weather metrics described in Section 2, and compare these annual average values with the annual average sunspot count, which is used to represent the 11-year solar cycle.

Figures 2(a) to 2(e) show the progression of the solar cycles (using the average sunspot number, the blue dashed curve), and the (a) Kp Index, (b) Dst Index, (c) AE index, (d) 10 MeV Proton Flux, and (e) $\log_{10}$ (1.8-3.5 MeV Electron Flux) for Solar Cycles 20–23 (1964 to 2008). These space weather indices are represented with a solid red curve. For the AE index, shown in Figure 2(c), data for 1976 is not available.

Figure 2(a) shows that from Solar Cycle 21 (1976 to 1986) onwards the Kp index lags behind the solar cycle, and generally reaches a maximum during the declining phase. As previously mentioned, the Kp scale goes from 0 (representing geomagnetically quiet activity) to 9 (intense geomagnetic activity), yet all of the Kp annual average values are less than 3.5. Thus, even near solar maximum the Kp index was relatively quiet during Solar Cycles 20 to 23.

Figure 2(b) shows the Dst along with the sunspot cycle. The Dst index is known as the best societal impact parameter for geomagnetic storms (Riley, 2012), but similar to Kp, it is difficult to analyse. Dst is primarily difficult because the average annual Dst fluctuates and contains outliers from geomagnetic storms. The scale of Dst becomes increasingly more negative during geomagnetic storms, with intense storms classified as Dst < –100 nT. Geogmanetic storms are most likely to occur during solar maximum, when coronal mass ejections (CMEs) that drive magnetic shocks and produce geomagnetic storms are most common (Mursula et al., 2008; Kamide et al., 1998). This is consistent with the annual average Dst data shown in Figure 2(b) which appears to have periods where Dst is more negative during solar maximum but the dependence is less clear than that of Kp index. This was also noted in Riley's (2012) analysis of elevated space weather events.

The AE index is known to significantly vary over short time scales, and therefore one should be take care in referencing the average AE index for a given period of time. Shown in Figure 2(c), the AE index appears to stay in phase with the sunspot curve after Solar Cycle 21. Data for the AE index is not available for 1977, so we do not include the ascending phase of Solar Cycle 21 in this study and a gap can be seen in Figure 2(c).

The annual average 10 MeV Proton flux curve, shown in Figure 2(d), fluctuates in phase with the solar cycle, increasing in magnitude during solar maximum, and decreasing in magnitude during solar minimum. The most noticeable increases during solar maximum were during Solar Cycles 20, 22, and 23, which increased to values between 40–55 pfu, respectively. The National Oceanic and Atmospheric Administration (NOAA), the entity responsible for broadcasting space environment warnings, alerts subscribers of 10 MeV proton flux measured greater than 10 pfu, 100pfu, 1,000 pfu, 10,000 pfu and 10,000 pfu, classified as S1–S5, respectively. Therefore, the maximum averages were considered to be S1 proton flux levels, which are considered minor with no biological effects or harm to satellite operations. However, these events may cause minor impacts on HF radio in the polar regions. The highest warning for 10 MeV protons is a flux of 10,000 pfu, and is considered to cause extreme biological effects (passengers and crew in high flying aircraft at high altitudes) and extreme effects to satellite operations (complete failures, memory impacts, permanent damage to solar arrays, etc.).

A description of the warning levels is provided at http://www.swpc.noaa.gov/NOAAscales/index.html#SolarRadiationStorms.

Figure 2 Annual mean values of the sunspot number (blue dashed curve) and annual averages of each dataset (solid red curve), for (a) Kp index, (b) Dst index, (c) AE index, (d) 10 MeV proton flux for Solar Cycles 20–23 (1964–2008), and (e) $\log_{10}$(1.8–3.5 MeV electron flux) (see online version for colours)

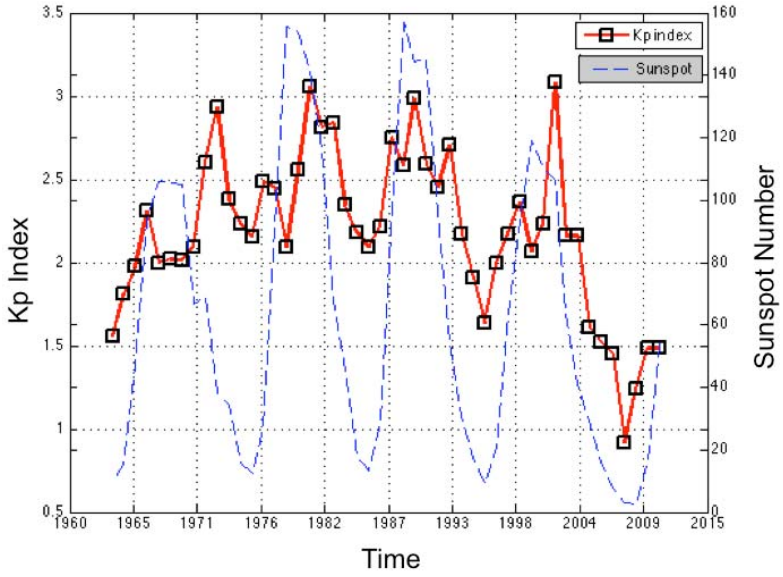

(a)

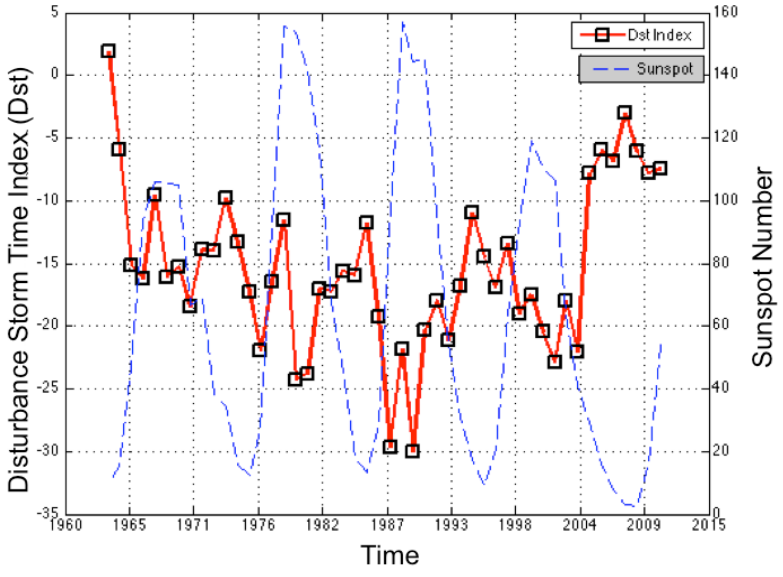

(b)

Figure 2 Annual mean values of the sunspot number (blue dashed curve) and annual averages of each dataset (solid red curve), for (a) Kp index, (b) Dst index, (c) AE index, (d) 10 MeV proton flux for Solar Cycles 20–23 (1964–2008), and (e) $\log_{10}$(1.8–3.5 MeV electron flux) (see online version for colours)

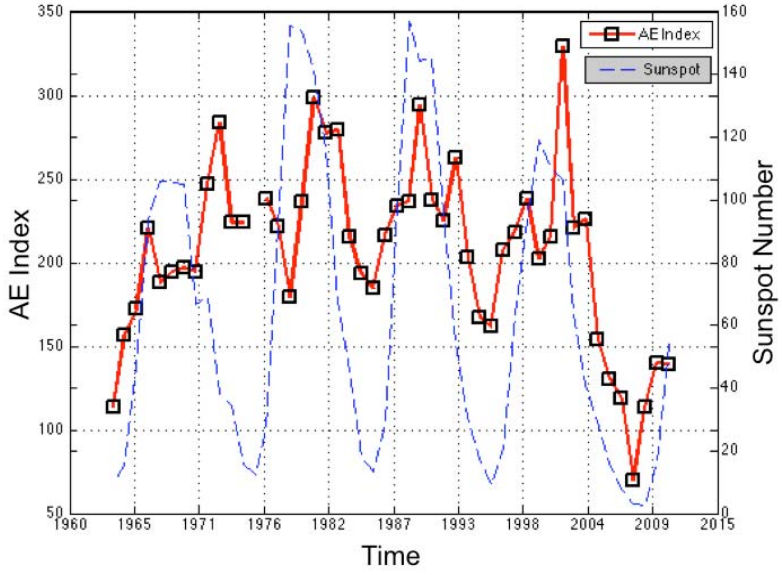

(c)

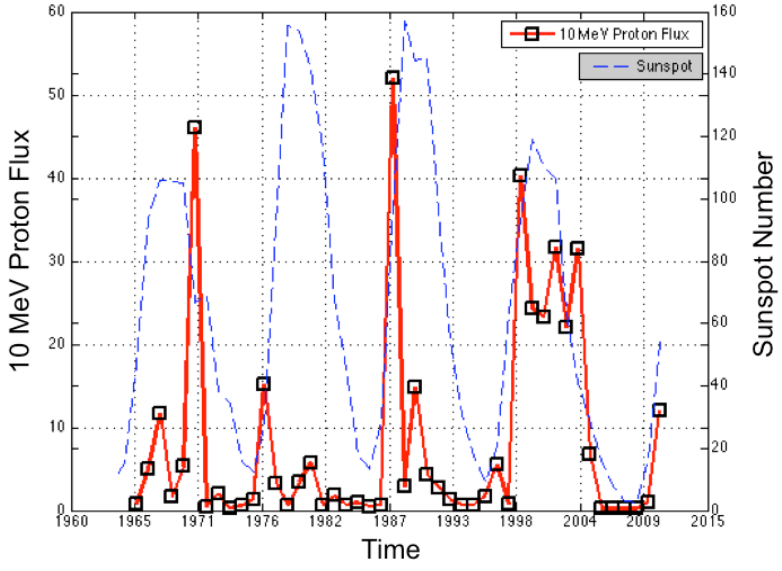

(d)

Figure 2 Annual mean values of the sunspot number (blue dashed curve) and annual averages of each dataset (solid red curve), for (a) Kp index, (b) Dst index, (c) AE index, (d) 10 MeV proton flux for Solar Cycles 20–23 (1964–2008), and (e) $\log_{10}$(1.8–3.5 MeV electron flux) (see online version for colours)

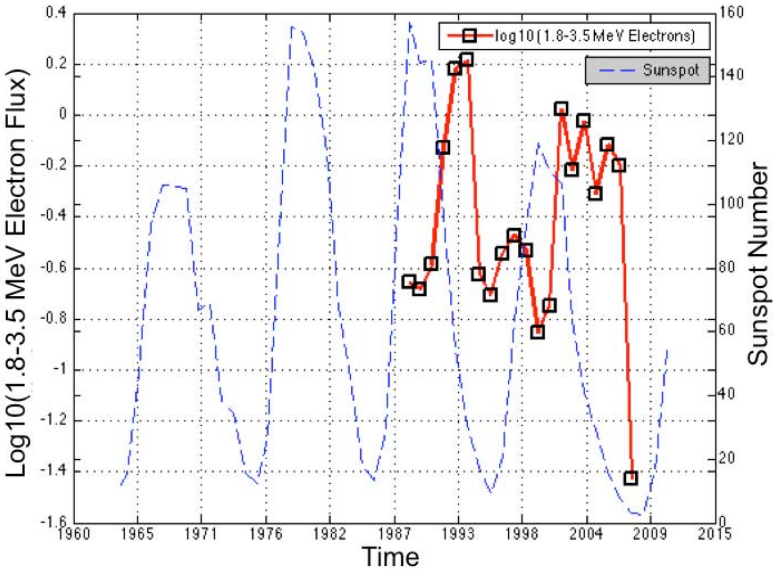

(e)

Figure 2(e) shows the solar cycle as well as the distribution of the annual averages of the LANL $\log_{10}$ (1.8–3.5 MeV electron flux) data. This dataset starts at Solar Cycle 22, and although it is much shorter in duration than the others, the $\log_{10}$ (1.8–3.5 MeV electron flux) curve appears to have a profile similar to Kp with maxima and minima that are slightly out of phase with the sunspot cycle, peaking during solar maximum.

4.2 Average values of space weather activity throughout Solar Cycle 20-23

The 'phase' of the solar cycle in which that satellite anomalies occur is often mentioned in investigation reports (e.g., solar maximum, declining phase of the solar cycle, etc.). To better understand how space weather activity varies throughout each of these cycles, we have calculated the average (mean) values of the five space weather metrics for the four different phases of a solar cycle for each of the Solar Cycles 20–23. These average values for each phase are tabulated in Tables 3 to 6. Note that the phases are not quite evenly divided into four per 11-year cycle as described in Table 2.

Figures 3(a) to 3(e) shows the mean values per phase of the solar sunspot cycle (blue dashed curve), and the (a) Kp index, (b) Dst index, (c) AE index, (d) 10 MeV proton flux, and (e) $\log_{10}$ (1.8–3.5 MeV electron flux) for Solar Cycle 20–23 (1964 to 2008). These mean values per phase are taken over the periods defined in Table 2. Extending the period over which the means are taken results in curves that have less variability than the annual means shown in Figures 2(a) to 2(e).

Figure 3 Mean values for the solar cycle (solid red curve), and (a) Kp index, (b) Dst index, (c) AE index, (d) 10 MeV proton flux for Solar Cycle 20–24 (1964–2008), and (e) $\log_{10}$(1.8–3.5 MeV electron flux) (see online version for colours)

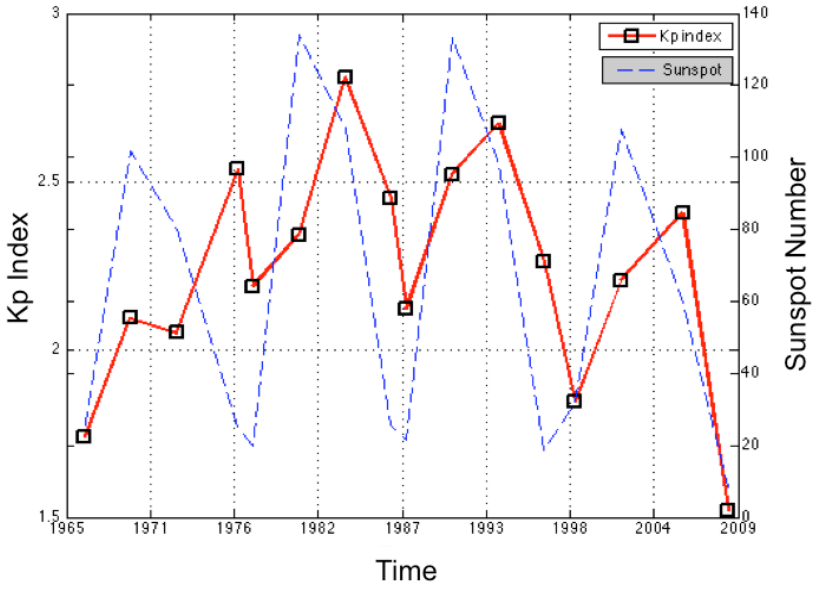

(a)

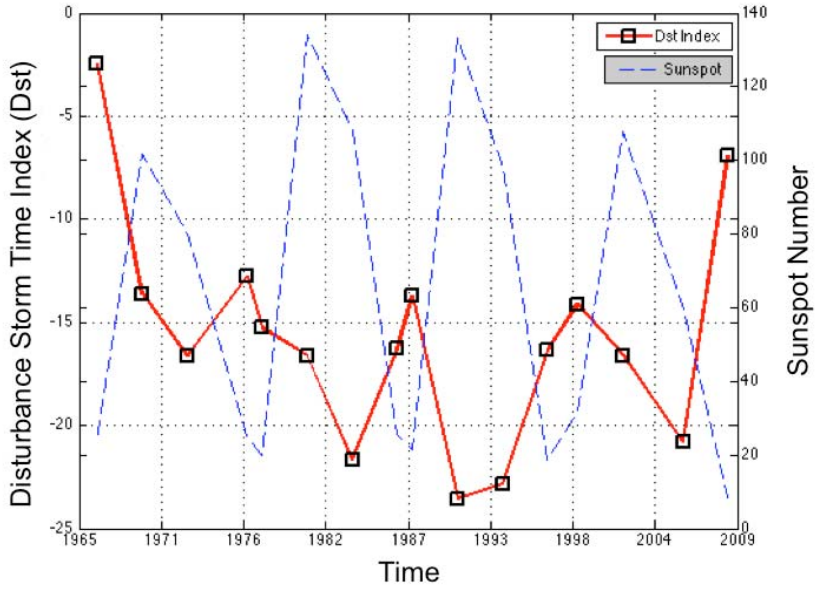

(b)

Note: These values are averaged over the periods defined in Table 2 (solar minimum, ascending, solar maximum, and declining phase).

Figure 3 Mean values for the solar cycle (solid red curve), and (a) Kp index, (b) Dst index, (c) AE index, (d) 10 MeV proton flux for Solar Cycle 20–24 (1964–2008), and (e) $\log_{10}$(1.8–3.5 MeV electron flux) (continued) (see online version for colours)

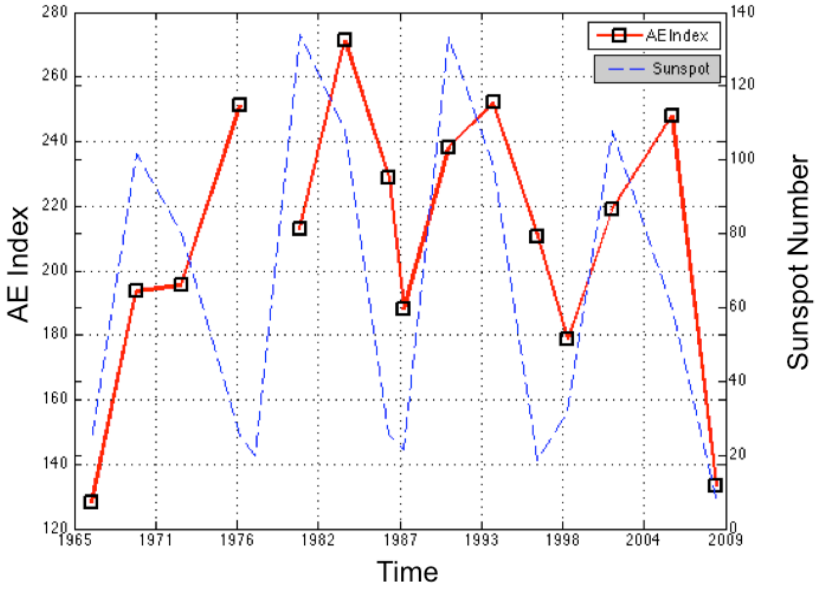

(c)

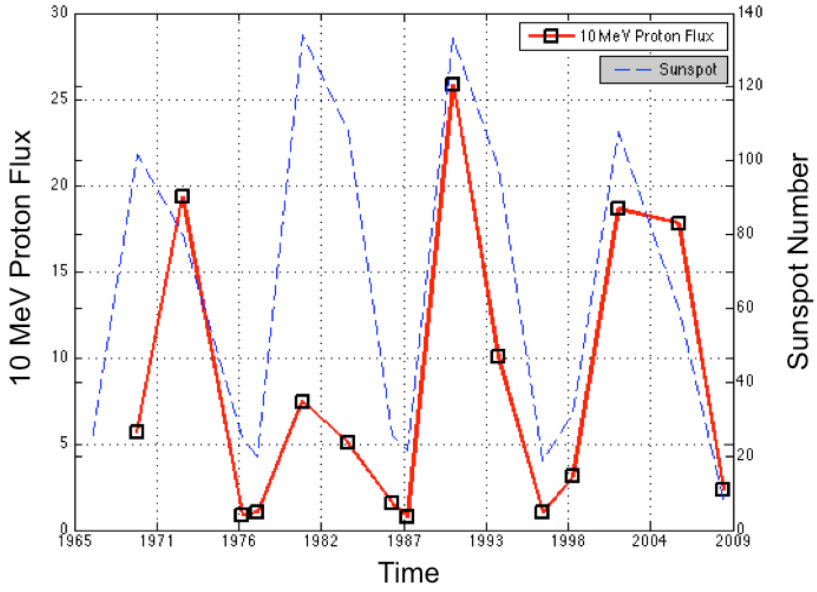

(d)

Note: These values are averaged over the periods defined in Table 2 (solar minimum, ascending, solar maximum, and declining phase).

Figure 3 Mean values for the solar cycle (solid red curve), and (a) Kp index, (b) Dst index, (c) AE index, (d) 10 MeV proton flux for Solar Cycle 20–24 (1964–2008), and (e) $\log_{10}$(1.8–3.5 MeV electron flux) (continued) (see online version for colours)

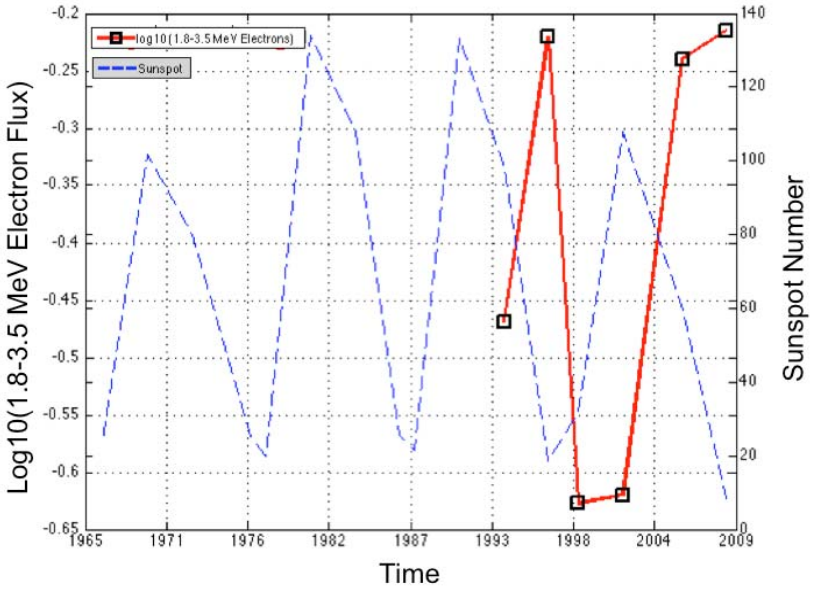

(e)

Note: These values are averaged over the periods defined in Table 2 (solar minimum, ascending, solar maximum, and declining phase).

4.3 Likelihood of increased space weather activity

Space weather forecasters analyse observational data and broadcast alerts to the community, such as commercial satellite operators, of approaching storms or potentially hazardous activity (O'Brien et al., 2013). While these space weather warnings are valuable, a more detailed understanding of the likelihood of hazardous space weather would aid the goal of a more causal and quantitative understanding of how the space environment relates to spacecraft anomalies. If a satellite operator systematically observes component anomalies occurring after increases in the space environment, then the environment could be a contributing factor to degraded satellite performance. In order to properly establish causality one must understand the definition of the typical space weather environment, how it fluctuates, and the likelihood of increases in the environment via the analysis of space weather metrics and in situ measurements.

Figure 4 The probability (%) that (a) Kp index, (b) Dst index, (c) AE index, (d) 10 MeV proton flux, and (e) $\log_{10}$ (1.8–3.5 MeV electron flux) exceeds greater than 2 MAD of the mean for each of the respective (a–e) space weather metrics for Solar Cycle 20–23 (see online version for colours)

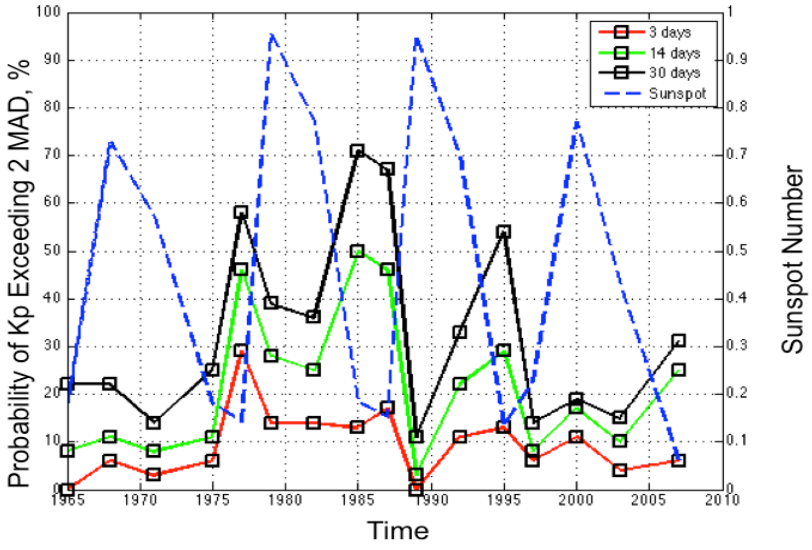

(a)

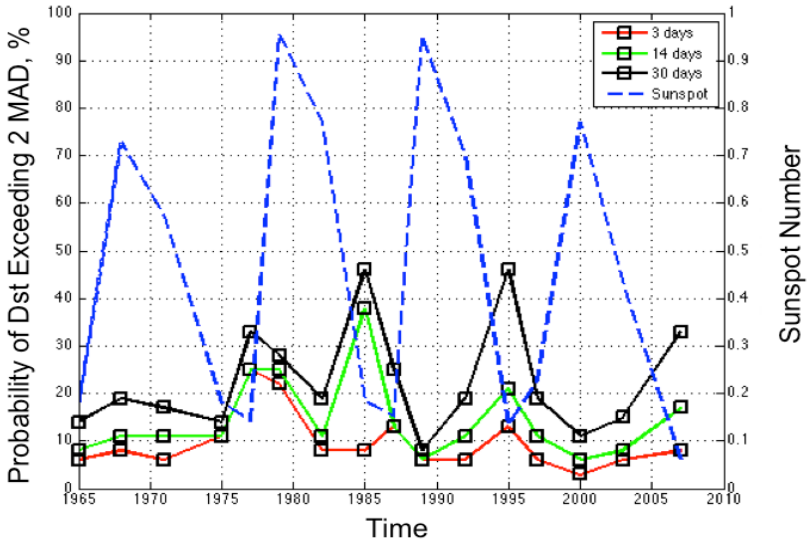

(b)

Notes: The blue dotted curves represent the sunspot number for Cycles 20–23. The red curve shows the likelihood that increased space weather activity occurs three days before the first day of each month, with 14 days shown in green and 30 days shown in black.

Figure 4 The probability (%) that (a) Kp index, (b) Dst index, (c) AE index, (d) 10 MeV proton flux, and (e) $\log_{10}$ (1.8–3.5 MeV electron flux) exceeds greater than 2 MAD of the mean for each of the respective (a–e) space weather metrics for Solar Cycle 20–23 (continued) (see online version for colours)

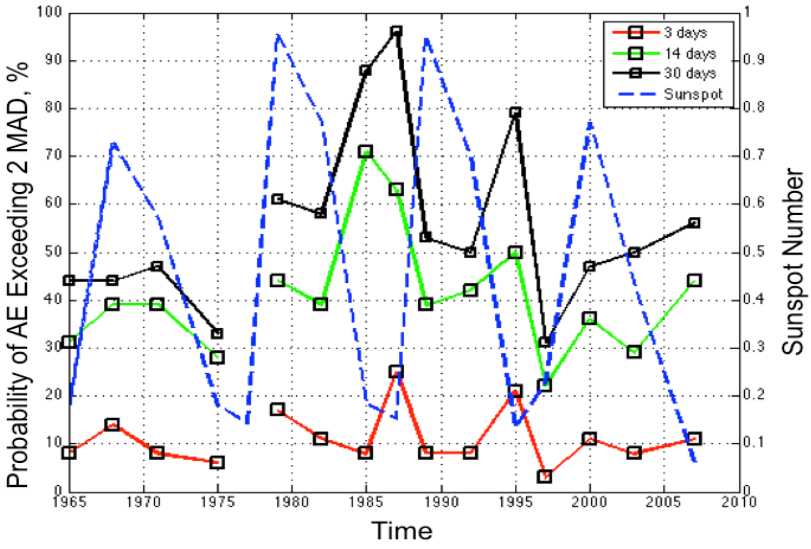

(c)

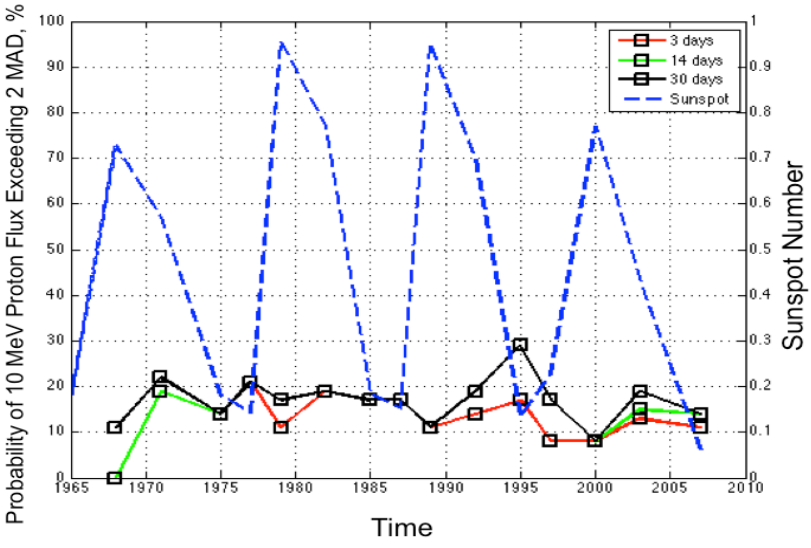

(d)

Notes: The blue dotted curves represent the sunspot number for Cycles 20–23. The red curve shows the likelihood that increased space weather activity occurs three days before the first day of each month, with 14 days shown in green and 30 days shown in black.

Figure 4 The probability (%) that (a) Kp index, (b) Dst index, (c) AE index, (d) 10 MeV proton flux, and (e) $\log_{10}$ (1.8–3.5 MeV electron flux) exceeds greater than 2 MAD of the mean for each of the respective (a–e) space weather metrics for Solar Cycle 20–23 (continued) (see online version for colours)

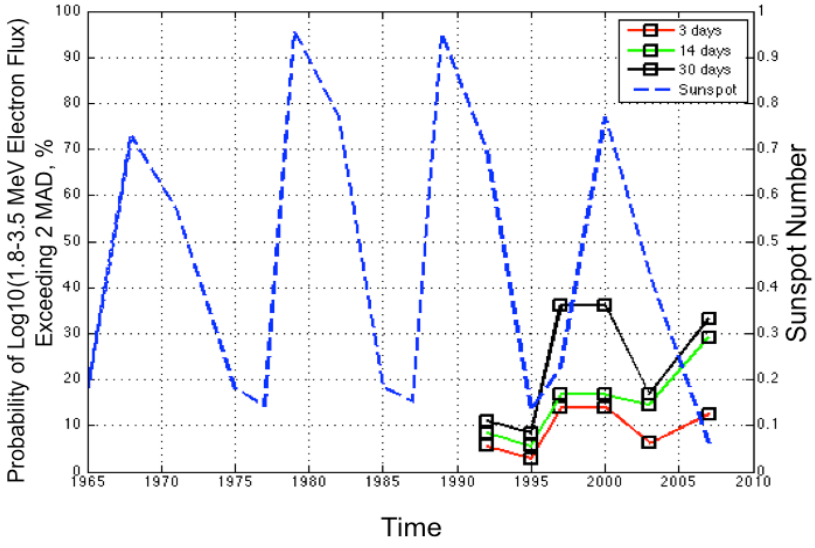

(e)

Notes: The blue dotted curves represent the sunspot number for Cycles 20–23. The red curve shows the likelihood that increased space weather activity occurs three days before the first day of each month, with 14 days shown in green and 30 days shown in black.

To understand the likelihood of increased space weather activity we calculate the probability that increased activity, defined as > 2 MADs of the mean of a given space weather metric, occurs before a specified time (three days, 14 days, and 30 days) of the first day of each month in a given portion of Solar Cycles 20–23. The first day of the month serves as a uniformly random selected day with respect to geomagnetic activity. The period of time over which the effects of the space environment could hinder satellite performance or potentially lead to a component anomaly is not well understood. Therefore, we explore three, 14 and 30 day periods to investigate near-daily, biweekly and monthly variability of the environment. If one were to determine the probabilities of increased space environment activity with respect to an average across the entire period of time (1963 to 2012), rather than on the smaller annual or 3–4 year solar cycle phase basis, the results would significantly differ, and in some cases by as much as 50%, substantially altering the understanding of the average space environment.

The values for both the means and the MADs are tabulated for the different phases of the solar cycle in Tables 3 to 6. Figures 4(a) to 4(e) show the probability of increased space weather activity for Solar Cycle 20–23 for periods of three days (red), 14 days (green), and 30 days (black).

4.3.1 Likelihood of increased Kp index

Figure 4(a) shows the probability (%) that the Kp index exceeds 2 MAD of the average Kp values for the respective phases of Solar Cycles 20–23. Figure 4(a) shows the variability of the Kp index, and reveals the complex nature of the metric. For these four solar cycles, the highest probability for increases in the Kp index above 2 MAD does not consistently occur for the same phase. From Figure 4(a), it can however be observed that increases in the Kp index, above the average Kp index for that phase, are generally most probably in the declining and minimum phase of the solar cycle.

To further elaborate, the maximum probability of Kp exceeding 2 MAD above the average Kp index for a given period in Solar Cycle 20 occurred at solar minimum and maximum for the 3-day average with a probability of 6%, likewise for the 14-day average with a probability of 11%, and during solar minimum for the 30-day average peaking at a probability of 25%. The maximum probability of Kp exceeding 2 MAD above the average Kp for Solar Cycle 21 occurred during the ascending phase for the 3-day average with a probability of 29%, and during solar minimum for the 14 and 30 day average with a likelihood of 50 and 71%, more than twice the maximum probability of Solar Cycle 20. The overall maximum probability of increased Kp occurred in the ascending phase of Solar Cycle 22, with a likelihood of 17%, 46%, and 67% for the 3-, 14-, and 30-day averages, nearly three times that of Solar Cycle 20. Solar Cycle 23 had similarities to Solar Cycle 20 with the highest probabilities of increased Kp occurring at solar maximum for the 3-day period (11%) and solar minimum for the 14-day (25%) and 30-day periods (31%).

4.3.2 Likelihood of increased Dst

The likelihood of increased Dst measurements is shown in Figure 4(b). The maximum probability of Dst measuring greater than 2 MAD of the average Dst for a given phase consistently occurred during the solar minimum phase for all four solar cycles. The probability reached as high as 46% for time periods of 30 days in Cycles 21 and 22, but did not exceed this value. We expected the maximum likelihood of increased Dst to occur at solar maximum, when the lowest and most extreme Dst measurements are typically recorded as shown in Figure 3(b). However, as tabulated in Tables 3 to 6, the average Dst for solar minimum and solar maximum are within 10 nT of each other for all four cycles, only a small amount of variability. In Solar Cycle 21, the average Dst for the solar maximum and solar minimum phase were even closer, within 1 nT of each other.

4.3.3 Likelihood of increased AE

Regions of enhanced conductivity at high latitudes provide a channel where magnetospheric currents can close in ionosphere. The ionospheric part of this closed current system is usually referred to as AE. The strength of this current as measured by AE index reflects the process in the magnetosphere including enhanced convection and substorm activity that can inject lower energy particles into the inner regions of magnetosphere. The maximum probability of increased AE measurements did not consistently fall in the same phase of each solar cycle. In fact, the maximum probability of increased AE occurred in a different phase for each of the solar cycles. This is most

likely due to the short-term variability of the AE metric is expected, as AE measures the convection in the space environment, which brings in low-energy electrons.

In Solar Cycle 20, the maximum probability occurred during solar maximum for the 3-day period and in the declining phase for the 30-day period. Also in Solar Cycle 20, for the 14-day period the maximum probability (39%) was equal for both the maximum and declining phases. Data for the year 1976 was not available, and therefore a gap in the curves exists during Solar Cycle 21. In the remaining phases of Solar Cycle 21, the maximum probability of increased AE occurred in solar maximum for 3-day periods and solar minimum for 14- and 30-day periods. In Cycle 22, the maximum likelihood of increased AE occurred during the ascending phase of the solar cycle for all periods, and peaked at 96% for a period of 30 days. For the last cycle considered, Solar Cycle 23, the highest probability of increased activity occurred during solar minimum.

4.3.4 Likelihood of increased 10 MeV proton flux

Figures 4(d) and 4(e) show the probability of increased 10 MeV proton flux, respectively. The probabilities for 10 MeV proton flux never exceed 30% for all time periods throughout the four solar cycles. The maximum probability of increased proton flux never occurred at solar maximum, but did occur in all other phases of the solar cycle. For Cycle 20 the maximum probability (between 17% to 22%) occurred during the declining phase. Solar Cycle 21 experienced a maximum probability of 21% for all time periods (3-days, 14-days, and 30-days) during the ascending phase of the cycle, and the maximum probability for Cycle 22 occurred during solar minimum. The maximum probability of increased proton flux for Cycle 23 occurred in all phases except for solar maximum.

4.3.5 Likelihood of increased $\log_{10}$ (1.8–3.5. MeV electron flux)

While the electron flux data was only obtained for 1.5 solar cycles, compared to four complete solar cycles for the metrics shown in Figures 4(a) to 4(e), Figure 4(e) shows the distribution of the probability of experiencing increased $\log_{10}$ (1.8–3.5 MeV electron flux) for Cycles 22 and 23, during the years 1989 to 2009. In Solar Cycle 22, probabilities were only obtained for the declining and minimum phases. The highest probability occurred during the declining phase and reached 11% for the 30 day time period, and as low as 5% for the 3-day time period before the first day of each month. Interestingly, the maximum probability of increased $\log_{10}$ (1.8–3.5 MeV electron flux) during Solar Cycle 23 occurred in all phases of the solar cycle, except for the declining phase when increases in high-energy electrons in the outer radiation belts occur (Li et al., 2005; Miyoshi and Kataoka, 2008). The maximum probability was 36% for a 30-day period before the first day of each month in the ascending and maximum phase of Cycle 23.

5 Summary and discussion

In this study, we analyse five space weather metrics and in situ measurements [Kp, AE, Dst, 10 MeV Proton flux and $\log_{10}$ (1.8–3.5 MeV electron flux)] throughout Solar Cycles 20–23 (1964 to 2008), and provide a reference for baselining how space weather

activity changes throughout the four phases of the solar cycle (maximum, descending, minimum, ascending). We do not attempt to determine the likelihood that these increases will cause satellite anomalies, but do discuss the potential consequences of increases in these metrics and in situ measurements.

We define the annual average value of each metric and the average value of each metric during the four phases of the solar cycles. If one were to determine the probabilities of increased space environment activity with respect to an average across the entire period of time (1963 to 2012), rather than on the smaller annual or 3–4 year solar cycle phase basis, the results would significantly differ, and in some cases by as much as 50%, substantially altering the understanding of the average space environment. For years 1963 to 2012, the average values of the five metrics and measurements over the entire period of time versus the averages over the individual phases of the four solar cycles between 1963 to 2012 differ by more than 28% for the Kp index, 37% for the AE Index, 84% for the Dst Index, and 200% for both the 10 MeV proton flux and $\log_{10}$ (1.8–3.5 MeV electron flux) measurements.

It is also often useful to check if a particular anomaly has been preceded by an anomalous increase in particle fluxes or space environment conditions as measured by geomagnetic indices. Such analysis is complicated by the fact that sudden increases preceding a particular anomaly may be simply a result of a coincidence. To perform analysis of sudden increase and determine if such increase can cause anomalies, it is most crucial to find the probability of such increase to occur for a random day. In this study, we choose the 1st of each month as a random day and calculated the probability. To that end, we calculate the MAD for each metric, and define increased space weather activity as greater than 2 MADs above the average activity for the particular phase of the solar cycle. Table 3 summarises the results tabulated in Table 3 to Table 6.

Using the calculated MADs we determine the probability that such increased values occur within 3-, 14- and 30 days before the first day of each month in the particular phase. Of the five metrics and in situ measurements we have identified that increases in Kp typically occur in the declining phase of the solar cycle, when the average Kp generally reaches a maximum. The declining phase is known to be potentially dangerous for satellite operations as geomagnetic activity is most active during this phase. However, periods of increased Kp have not been found to correlate with satellite anomalies, and therefore when characterising the environment from a hazard perspective the Kp metric should be considered in combination with other metrics and in situ measurements.

The maximum probability of increased AE does not occur consistently in a particular phase, but did reach the highest probability of all five metrics, 96%, during the ascending phase of Solar Cycle 22. The fact that the maximum probability of increased AE occurred in a different phase for each of the solar cycles is most likely due to the sporadic, variable nature of the metric. With respect to satellite anomalies, AE shows the conductivity of the space environment, which can be used as a proxy for low-energy electrons that could potentially contribute to surface-charging related anomalies or ESD arcs on solar arrays.

The Dst index is used to measure the severity of geomagnetic storms, which are most common during solar max. The scale of Dst is most negative when geomagnetic storms are present, and therefore the lowest values of Dst are found to occur at solar maximum. However, we find that the maximum likelihood of increased Dst always occurs during solar minimum. Again, the maximum likelihood of increased Dst does not insinuate the maximum values of Dst, or the most severe geomagnetic storm, but that increases greater

than 2 MAD are most likely to occur. This does not necessarily have hazard implications for satellite operations, but geomagnetic storms are known to effect satellite performance.

As shown in Table 3, the average 10 MeV proton flux behaviour was consistently low throughout the cycles, ranging from 0.735 to 25.849. Flux values of this level (~10 pfu) are considered the lowest class, S1, for which NOAA broadcasts warnings. High-energy protons are known to peak at solar maximum, and are notoriously known to cause solar array degradation and single event effects. The probabilities for 10 MeV proton flux increasing above 2 MAD never exceed 30% for all time periods (3 days, 14 days and 30 days) throughout all four solar cycles, and maximum probability of proton flux above 2 MAD never occurred in the solar maximum phase, but did occur in all other phases of the solar cycle. While this may seem contradictory, it simply means that fluxes are steadier during times when fluxes are elevated.

The average annual flux and average phase electron flux, shown in the Figures 2(e) and 3(e), respectively, reach maximum flux during the declining phase of the solar cycle, which is known as phase when elevated high-energy electrons in the outer radiation belts occur (Li et al., 2005; Miyoshi and Kataoka, 2008). The declining phase is considered particularly hazardous for satellite operations with respect to high-energy electron induced internal charging of dielectric components. The $\log_{10}$ (1.8–3.5 MeV electron flux) data is only present for 1.5 solar cycles (half of cycle 23 and all of solar cycle 24), yet we find that the likelihood of increased $\log_{10}$ (1.8–3.5 MeV electron flux) occurs in the declining phase of Cycle 22 and the minimum phase of Cycle 23.

The approach and results of this study provide greater insight for the satellite operator and engineering community into baselining how space weather activity changes throughout the solar cycle. Understanding whether sudden jumps in a given metric are typical for a particular phase of the solar cycle is particularly useful for satellite operators responsible for monitoring the performance and component health of spacecraft throughout the duration of the mission (e.g., launch, manoeuvres, etc.), and aids in determining the contribution of the environment on satellite component anomalies.

References

Allen, J. (2010) 'The Galaxy 15 anomaly: another satellite in the wrong place at a critical time', *Space Weather*, Vol. 8, No. 6, p.S06008, DOI: 10.1029/2010SW000588.

Baker, D.N. (2000) 'The occurrence of operational anomalies in spacecraft and their relationship to space weather', *IEEE Transactions on Plasma Science*, Vol. 28, No. 6, pp.2007–2016, DOI: 10.1109/27.902228.

Baker, D.N. (2002) 'How to cope with space weather', *Science*, Vol. 297, No. 5586, pp.1486–1487, DOI: 10.1126/science.1074956.

Bodeau, M. (2010) 'High energy electron climatology that supports deep charging risk in GEO', *paper presented at 48th AIAA Aerospace Sciences Meeting Including the New Horizons Forum and Aerospace Exposition*, Orlando, FL, 4–7 January.

Clette, F., Berghmans, D., Vanlommel, P., Van der Linden, R.A.M., Koeckelenbergh, A. and Wauters, L. (2007) 'From the Wolf number to the International Sunspot Index: 25 years of SIDC', *Advances in Space Research*, Vol. 40, No. 7, pp.919–928, DOI: 10.1016/j.asr.2006.12.045.

Draghici, S. (2001) 'Data analysis tools for DNA microarray data', Paper presented at the *Pacific Symposium on Biocomputing 2001*, Hawaii, HI, 3–7 January.

Fennell, J.F., Koons, H.C., Roeder, J.L. and Blake, J.B. (2001) 'Spacecraft charging: observations and relationships to satellite anomalies', Aerosp. Rep. TR-2001(8570)-5, Aerosp. Corp., Los Angeles, California.

Gonzalez, W.D., Joselyn, J.A., Kamide, Y., Kroehl, H.W., Rostoker, G., Tsurutani, B.T. and Vasyliunas, V.M. (1994) 'What is a geomagnetic storm?', *Journal of Geophysical Research*, Vol. 99, No. A4, 5771–5792.

Horne, R.B., Glauert, S.A., Meredith, N.P., Boscher, D., Maget, V., Heynderickx, D. and Pitchford, D. (2013) 'Space weather impacts on satellite and forecasting 1 the Earth's electron radiation belts with 2 SPACECAST', *Space Weather*, DOI: 10.1002/swe.20023.

Iucci, N., Dorman, L.I., Levitin, A.E., Bevlov, E.A, Eroshenko, N.G., Villoresi, G., Chizhenkov, G.V., Gromova, L.I., Parisis, M., Tyasto, M.I. and Yanke, V.G. (2006) 'Spacecraft operational anomalies and space weather impact hazards', *Advances in Space Research*, Vol. 37, No. 1, pp.184–190, DOI: 10.1016/j.asr.2005.03.028.

Kamide, Y. and Akasofu, S. (1983) 'Notes on the Auroral Electrojet indices', *Reviews of Geophysics and Space Physics*, Vol. 21, No. 7, pp.1647–1656.

Kamide, Y., Baumjohann, W., Daglis, I.A., Gonzalez, W.D., Grande, M., Joselyn, J.A., McPherron H.L., Philips, J.L., Reeves, E.D.G., Rostoker, G., Sharma, A.S., Singer, H.J., Tsurutani, B.T. and Vasyliunas, V.M. (1998) 'Current understanding of magnetic storms: storm-substorm relationships', *Journal of Geophysical Research*, Vol. 103, No. A8, pp.17705–17728.

Kane, R.P. (2002) 'Some implications using the group sunspot number reconstruction', *Solar Physics*, Vol. 205, No. 2, pp.282–401.

King, J. and Papitashvili, N. (2013) *OMNI 2 Preparation*, Goddard Spaceflight Center archives [online] http://omniweb.gsfc.nasa.gov/html/omni2_doc_old.html (accessed 1 October 2012).

Li, X., Baker, D.N., Temerin, M., Reeves, G., Friedel, R. and Shen, C. (2005) 'Energetic electrons, 50 keV to 6 MeV at geosynchronous orbit: their responses to solar wind variations', *Space Weather*, Vol. 3, No. 4, p.S04001, DOI: 10.1029/2004SW000105.

Miyoshi, Y. and Kataoka, R. (2008) 'Flux enhancement of the outer radiation belt electrons after the arrival of stream interaction regions', *Journal of Geophysical Research*, Vol. 113, No. A3, p.A03S09, DOI: 10.1029/2007JA012506.

Mursula, K., Holappa, L. and Karinen, A. (2008) 'Correct normalization of the Dst index', *Astrophysics and Space Sciences Transactions*, Vol. 4, No. 2, pp.41–45.

Neil, T. and Sugiura, M. (1966) 'Auroral electrojet activity index AE and its universal time variations', *Journal of Geophysical Research*, Vol. 71, No. 3.

O'Brien, T.P. (2009) 'SEAES-GEO: a spacecraft environmental anomalies expert system for geosynchronous orbit', *Space Weather*, Vol. 7, No. 9, p.S09003, DOI: 10.1029/2009SW000473.

O'Brien, T.P., Mazur, J.E. and Fenell, J.F. (2013) 'The priority mismatch between space science and satellite operations', *Space Weather*, Vol. 11, No. 2, p.49, DOI: 10.1002/swe.20028.

Reeves, G.D., Morley, S.K., Friedel, R.H.W., Henderson, M.G., Cayton, T.E., Cunningham, G., Blake, J.B., Christensen, R.A. and Thomsen, D. (2011) 'On the relationship between relativistic electron flux and solar wind velocity: Paulikas and Blake revisited', *J. Geophys. Res.*, Vol. 116, No. A2, p.A02213, DOI: 10.1029/2010JA015735.

Riley, P. (2012) 'On the probability of occurrence of extreme space weather events', *Space Weather*, Vol. 10, No. 2, pp.1–12, DOI: 10.1029/2011SW000734.

Russell, C.T. and McPherron, R.L. (1973) 'Semiannual variation of geomagnetic activity', *J. Geophys. Res.*, Vol. 78, No. 1, pp.92–108, DOI: 10.1029/JA078i001p00092.

Shea and Smart (1998) 'Space weather: the effects on operations in space', *Advances in Space Research*, Vol. 22, No. 1, pp.29–38.

Thomsen, M.F. (2004) 'Why Kp is such a good measure of megnetospheric convection', *Space Weather*, Vol. 2, No. 11, pp.1–10, DOI: 10.1029/2004SW000089.

Vaquero, J.M. (2007) 'Historical sunspot observations: a review', *Advances in Space Research*, Vol. 40, No. 7, pp.929–941, DOI: 10.1016/j.asr.2007.01.087.